DOI: https://doi.org/10.5592/CO/EUROENGEO.2024.165

CORRELATING THE SPATIAL DISTRIBUTION OF LIQUEFACTION PHENOMENA WITH THE SURFICIAL GEOLOGY ON POINT BARS DEPOSITS; CASE STUDIES 2021 DAMASI, GREECE AND 2023, KAHRAMANMARAŞ, TÜRKIYE

MARIA TAFTSOGLOU[1], SOTIRIS VALKANIOTIS[1], GEORGE PAPATHANASSIOU[2], VASSILIS NTOUVARTZIS[2], DIMITRA RAPTI[3], RICCARDO CAPUTO[4]

[1] *Dept. Civil Engineering, Democritus University of Thrace, Greece,* mtaftsog@civil.duth.gr, svalkani@civil.duth.gr

[2] *School of Geology, Aristotle University of Thessaloniki, Greece,* gpapatha@geo.auth.gr, vasintou@geo.auth.gr

[3] *Dept. Chemical, Pharmaceutical and Agricultural Sciences, Ferrara University, Italy,* dimitra.rapti@unife.it

[4] *Dept. Physics and Earth Sciences, Ferrara University, Italy,* rcaputo@unife.it

Abstract

Liquefaction, a seismic threat to critical infrastructure, demonstrated its impact in the 2021 Damasi event in Greece and the 2023 Türkiye events. In both cases, extensive liquefaction phenomena were triggered in the floodplain and point bars of large meandering rivers. Considering that the identification of the paleoenvironmental features is a crucial step to assess the liquefaction susceptibility of an area, this research aims to statistically investigate the spatial distribution of liquefaction within point bars. Using historical and contemporary data, we were able to reconstruct the evolution of meandering fluvial systems in both cases and preliminary delineate the different types of lithofacies encountered in point bars; sand and mud prone. Afterwards, we compared the location of liquefaction related phenomena, ejecta and lateral spreading, with the predominant type of soil material within the point bars. As an outcome, it was concluded that more than 80% of the liquefaction phenomena, triggered by these two earthquake cases, reported on the upstream flow direction of point bars which is characterized as sandy like zone.

Key words

Liquefaction, point bar, lithofacies, geomorphology, remote sensing

1 Introduction

The occurrence of liquefaction phenomena and the induced failures are crucial issues that shoud be taken into account to ensure the stability of manmade structures and lifelines. During the last decade, major earthquakes in New Zealand, Italy, Greece and Türkiye demonstrated the severity of the liquefaction-induced damages. The outcomes that arose from these devoted studies strengthened the opinion that spatial distribution of these phenomena follows defined patterns and is strongly correlated with the depositional history of the sediments (Wotherspoon et al., 2012, Di Manna et al., 2012, Bastin et al., 2015, Papathanassiou et al., 2012; 2015; 2022, Civico et al., 2015, Taftsoglou et al., 2023, Abayo et al., 2023). In several cases it was concluded that most of the liquefaction effects were not randomly distributed over a floodplain but were concentrated in specific geomorphological areas where fine- and coarse-grained sediments of Holocene age sorted by fluvial or wave actions are deposited. In particular, old/ abandoned channels, point bars and coastal formations exhibited a notably higher density in liquefaction occurrences than other parts of a floodplain. Consequently, the reliability of a liquefaction susceptibility map is highly dependent by the scale and accuracy of the geological and geomorphological mapping of a floodplain.

Aiming to delineate the prone to liquefaction areas, many researchers used remote sensing techniques for compiling geomorphological maps (Papathanassiou et al., 2022, Taftsoglou et al., 2022; 2023).Thus,

the more likely to liquefaction geomorphological features are traced in detail, leading to a more reliable liquefaction susceptibility map.
Following this approach, this research focuses on the valleys of Piniada in Thessaly (Greece) and Orontes in Hatay (Türkiye), where the mainshocks of Mw=6.3 on 2021 and Mw=7.7 on 2023 occurred, respectively. As both valleys are covered by Quaternary fluvial deposits of Pinios and Orontes rivers, particular emphasis were placed on point bar formations where liquefaction phenomena i.e.ejecta and lateral spreading, were triggered by these two events. Taking into account the heterogeneity of the non-cohesive material accumulated on the inner part of the meander (point bars), the relationship between the distribution of liquefaction sites and the sand- and mud-prone sediments were examined. The delineation of different types of lithofacies was achieved by applying the method proposed by Russel et al., (2017) and correlated with the spatial distribution of manifestation with the predominant type of soil material, resulted to the evaluation of the total liquefaction density per heterogeneity type. As an outcome, it was concluded that most of liquefaction phenomena, triggered by these two earthquake cases, were triggered on the upstream flow direction of point bars, characterized as sandy like zone.

1.1 The case study of 2021 Damasi, Greece

On March 2021, a seismic sequence occurred in Thessaly, Central Greece, characterized by a Mw= 6.3 mainshock close to Damasi village and five Mw > 5.0 aftershocks. Considering the post earthquake documentation, extensive liquefaction manifestations were triggered in the floodplain of the Piniada Valley.
Defined as the central reach of Pinios River, Piniada Valley is located in between the western Karditsa and Eastern Larissa plain and represents an area of significant anomaly of the hydrographic network, as far as it allows the connection between these two basins since Early Quaternary age (Caputo et al., 2021). During the Late Quaternary, Piniada Valley was progressively filled by marshy-lacustrine deposits and finally by the eastwards prograding internal deltas of the Pinios River (Caputo et al., 2021). As a result of this complex geological evolution, the current Piniada Valley is characterized as an alluvial plain entirely covered by fluvial formations of abandoned channels, point bars and floodplain deposits (Fig.1). Documentation of liquefaction manifestations in Piniada Valley reported a 26.7m ground fissure as the longest one, while the total coverage of ejecta material was estimated as 0.0325 km^2 (Papathanassiou et al., 2022). Following the detailed geological mapping and the statistical analyses of the spatial distribution of liquefaction phenomena with the geomorphological features, it was shown that most of the liquefaction effects concentrated within specific areas that correspond to deposits formed as point bars and filled abandoned channels.

1.2 The case study of 2023 Türkiye earthquakes

During the 2023 earthquake doublet of Mw 7.7 and Mw 7.6 on East Anatolian Fault Zone (EAF), extensive liquefaction was observed at Amik Valley and specifically in Orontes (Asi) River. Being infilled with Plio-Quaternary sediments of more than 200–300 m thickness, Amik Plain extends for approximately 36 km long and 40 km wide and its drainage is controlled by Orontes, Karasu, and Afrin Rivers from the south, north, and east, respectively. In the past, the western central part of this valley was covered by Amik Lake, where through the last decades was completely drained by an artificial channel system into the Orontes River (Hazir et al., 2016).
As one of the most affected regions, due to liquefaction phenomena after the 2023 seismic events, Orontes River Valley presented a significant number of 560 sites of ejecta and lateral spreading effects in its meandering, delta and open valley zones (Taftsoglou et al., 2023).
For the purposes of this study, we focused on a segment of Orontes close to the South-East part of Amik Valley, delineating more than 0.161 km^2 of ejecta material and 0.544 km^2 of lateral spreading phenomena (Fig.2).

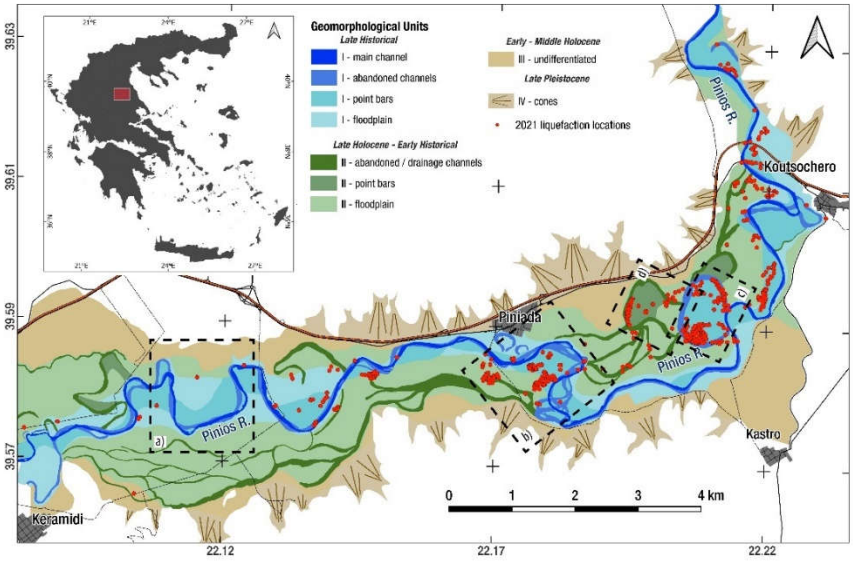

Figure 1. Surface geological map of the Piniada Valley-modified after Valkaniotis et al.(2024, in review). Red dots showing the liquefaction sites. Indexes (a-d) represent meanders where Russell criteria were applied.

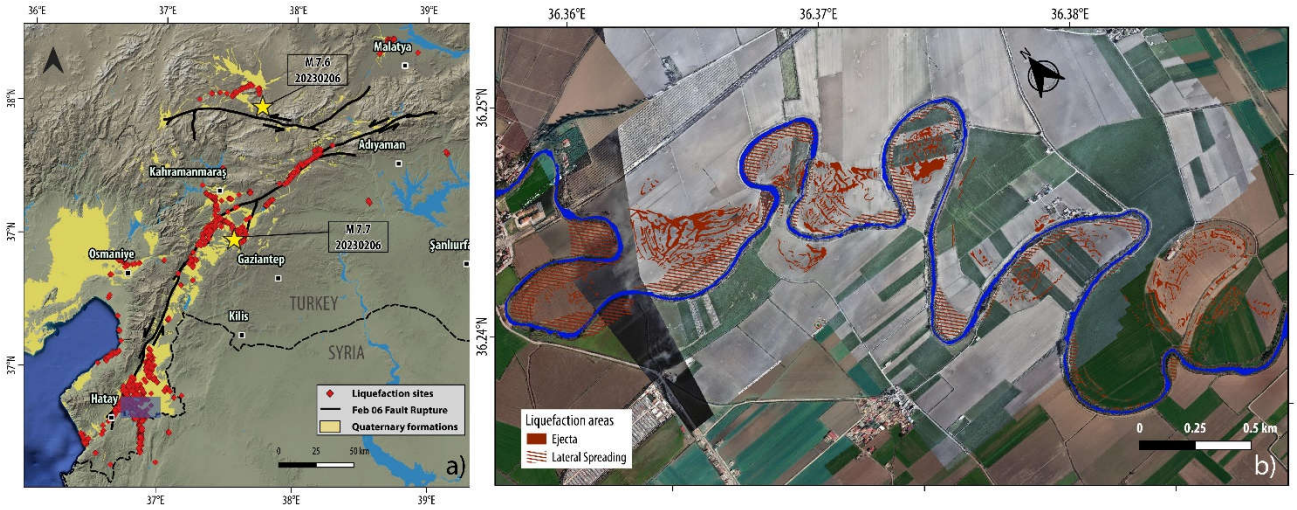

Figure 2. (a) Overview map of liquefaction and lateral spreading sites of the 2023 Türkiye / Syria earthquakes, identified and mapped using satellite imagery (Taftsoglou et al., 2023). Blue box indicates the area of figure b. (b) Liquefaction areas of ejecta and lateral spreading in the study area.

2 Methods

For the purposes of this study, the method proposed by Russell (2017) was applied for the cases of point bars at Piniada and Orontes Valley. Russel (2017) suggested that point-bar deposits are laterally discontinuous (Allen, 1965) and characterised by a complex distribution of lithofacies (Thomas, 1987, Tye, 2004, Miall, 2006, Durkin et al., 2015) comprised by alterations of mudstone and sandstone beds, while their sedimentology is strongly correlated with the evolution of a meander system and variations in channel geometry, channel orientation and channel position.

In addition, according to previous studies, the grain size of the deposited material in point-bar formations is influenced by the flow direction and speed of the meander, with the deposition of the finer grained materials occurs mostly in the downstream part and coarser deposits in the upstream part (Jackson, 1976, Fustic et al., 2012, Nardin et al., 2013). Furthermore, calibre of the sediment in a meander bend is

influenced by the different meander growth stages (expansion, translation and rotation), expressed as scroll bar morphologies and composed of genetically related sediments (Ghinassi et al., 2006). Furthermore, Smith et al., (2009) stated that when accretion occurs on the outer bank of meander, calibre of sediment may fine upstream, due to turning of scroll bars from concave to convex shapes and formation of the counter point-bar morphologies. Thus, counter point-bars can display the transition between the mud-prone and sand-prone beds.

In order to apply the methodology proposed by Russell et al., (2017), it is required to initial measure the meander shape and the episodes of meander growth in point bars features. In particular, it was measured the meander apex, the division of meander into the upstream and downstream part, the projection of the thalweg lines, the width of meander bend (mW) and the migration trajectory (tL) where scroll bars were visible. It should be noted that tracing of different meander generations was achieved in both cases using very high-resolution satellite images dated close to the seismic events (2021 and 2023), while in case of Piniada Valley 1945 historical aerial imagery was also used.

Through the first phase, the meander shapes developed after different growth stages were classified based on their geometrically shapes into four groups of 25 individual shapes: open asymmetric, angular, bulbous, open symmetric. Afterwards, thalweg line and apex for each meander were drawn separately, while locations in the downstream limbs where a riffle or cross-over once existed were characterized as inflection points and represented the transitional zones from sand- to mud-prone sediments (Smith et al., 2009).

Through the next step, meander thalweg lines were subdivided to heterogeneity types of Sand-I, Sand-II, Mud-I, Mud-II, according to the relative proportion of coarse to fine-grained material. Generally, for the open asymmetric, angular and open symmetric groups, Sand-I is mostly recorded on the upstream part, while Sand-II deposition occur after the upstream cross-over with its deposition influenced by the geometry and the growth of the meander. Sediments of Mud-I and Mud-II are mostly concentrated in downstream limbs, where counter point bars transforming from concave to convex forms. By contrast with the aforementioned groups, bulbous shaped meanders forming more than two inflection points and consequently can compound multiple zones of all relative heterogeneity types (Carter, 2003, Nanson et al., 1980). Combining this data with the ones regarding the direction or shifting of scroll bars and cross-cutting relationships, resulted in the compilation of a map for each investigated meander showing their relative heterogeneity types.

Having delineated the heterogeneity of point bars and compiled the relevant map, the liquefaction phenomena of ejecta and lateral spreading for Piniada and Orontes Valleys were plotted on these maps and correlated with the different lithofacies. In particular, the liquefaction density per heterogeneity type of sediment was calculated. In addition, it was investigated the correlation between the maximum distance of lateral spreading, from the free faces, with the different lithofacies of point bars.

3 Results

In order to examine the correlation between the density of liquefaction phenomena and the distribution of sand and mud rich deposits, we initially delineated the different lithofacies on selected point bars in Piniada and \ in Orontes Valley. For the purposes of this study three cases for both areas are discussed through the following paragraphs and the results are presented in Table 1 and Table 2.

The first examined meander of Piniada Valley is close to the Piniada village. Based on the 1945 historical aerial imagery, the delineated meander shape was classified as a compound of two distinct meanders of open asymmetric (S1i) and angular (S2c) type (a in Fig.3). According to the 2021 satellite image, the previous compound meander was transformed into a bulbous shape type (S3e) where four heterogeneity classes were traced after the projection of 1945 and 2021 heterogeneity thalweg lines. Following the 2021 earthquake sequence, liquefaction phenomena covered the coarser deposits of the upstream limb, with a number of 63.6% of the total records.

The second examined meander of Piniada valley is a cut-off form (b in Fig.3), which according to historical aerial imagery of 1945 was classified as a bulbous meander with a rounded apex and not overturned shape (S3a). Moreover, scroll bar morphologies indicated an extensional and rotational meander growth, where more than one major directional change occurred. However, due to the abandoned form of this meander since 1945, no alterations were detected in the recent 2021 image. Based on the 2021 liquefaction mapping, more than 70% of liquefaction sites was observed in areas of coarser material, with 63.3% and 9.4% corresponding in Sand-I and Sand-II types respectively.
The third area of interest in Piniada Valley is related to a cut-off meander (c in Fig.3) formed next to the previous one. Characterised as older cut-off feature, it was analysed separately and classified as an asymmetrical bulbous type (S3e). Regarding the liquefaction phenomena reported in this zone, post-event field observations document that the higher concentration of 87.5% was related to the area considered as Sand-II type.

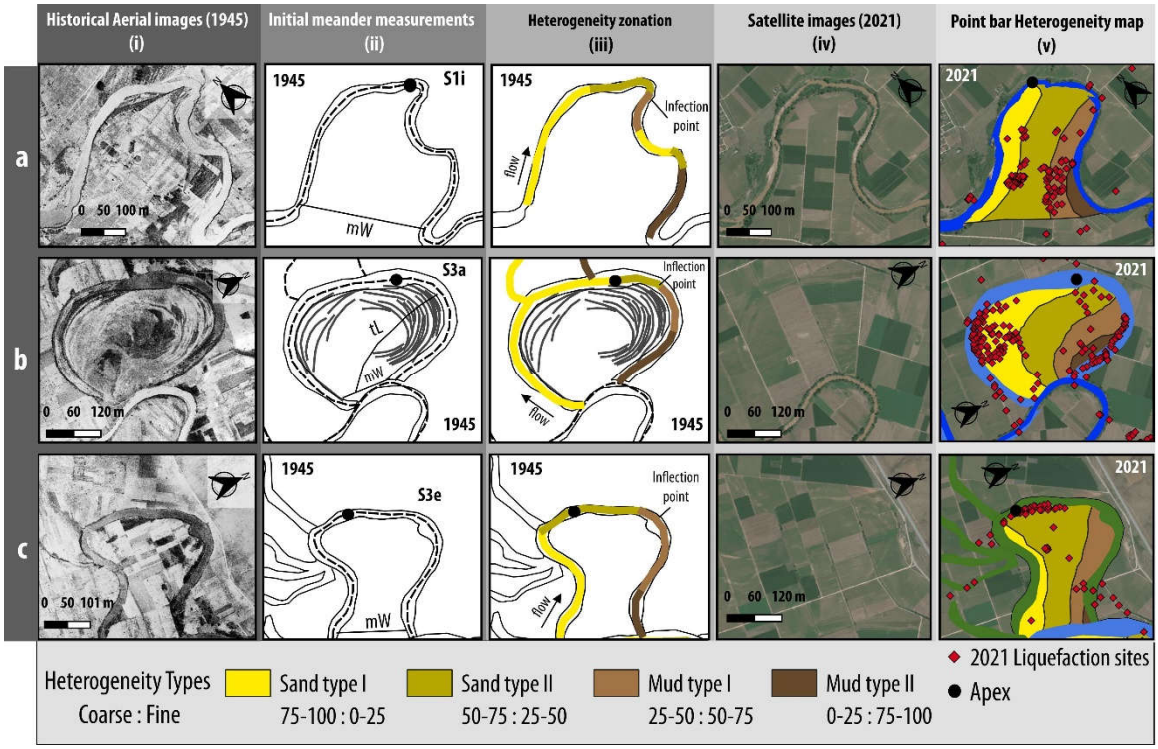

Figure 3. Assessment of heterogeneity types in four selected meanders (a-c) of the Piniada Valley based on the methodology proposed by Russell (2017) Columns (i-v) represent the different steps of the procedure for evaluating the sedimentary heterogeneity due to the Pinios River evolution from 1945 to 2021. Abbreviations of measurements in column (ii) stand for meander width (mW) and meander trajectory length (tL), while codes attributed to each meander shape refer to meander shape (S); parent group to which the meander belongs (1: open asymmetric, 2: angular, 3: bulbous, 4: open symmetric) and further qualifications of the meander shape ("a" to "i") (from Valkaniotis et al., 2024, in review, modified for the purposes of this study)

Following the same procedure with Piniada Valley, we focused on a segment of Orontes river close to the South-East part of Amik Valley. The delineated meander of first case (a in Fig.4) was classified as a bulbous shape (S3a). Tracing of the heterogeneity types in the thalweg of 2023 resulted in a map of four heterogeneity classes, with coarser materials covering the upstream limb and the areas of both apex, and finer sediments extending in the downstream part. According to the 2023 liquefaction manifestations, ejecta materials were detected only in Sand-I and Sand-II types (69.5% and 30.5%

respectively), while 82.2% of lateral spreading phenomena were observed in the same deposits (Table 1).

The second case study in Orontes river was also classified as a bulbous overturned shape (S3b) (b in Fig.4). Due to the projection of two downstream inflection points, the zonation of meander thalweg into heterogeneity types resulted in a map of multiple relative heterogeneity classes. Projection of liquefaction sites show that 40.2% and 51.6% of ejecta materials were detected in Sand-I and Sand-II deposits respectively.

Finally, the third case is a cut-off meander characterised as a bulbous shape with a rounded apex and an asymmetrical form (S3d) (c in Fig.4). Based on the 2023 satellite image, tracing of the heterogeneity types in the meander's thalweg classified the area into three heterogeneity classes of Sand-I, Sand-II and Mud-I. After the 2023 seismic events, 45.8% of the total ejecta material were detected mostly in the Sand-II deposits, while in this case 30.7% was found in Mud-I type.

Consequently, based on the analysis that took place in this study, most of liquefaction phenomena triggered by 2021 Damasi earthquake and 2023 Türkiye earthquakes are correlated with areas characterised as Sand-I and Sand-II types. As shown in Table 1, 72.7% of the total liquefaction sites in Piniada Valley were detected in sand prone zones, with the highest percentage concentrated in sediments of Sand-I type (38.4%). On the other hand, most of the liquefaction ejecta areas of Orontes case were hosted in the Sand-II material (62.7%).

Regarding the lateral spreading phenomena, 80.6% of them were recorded in the coarser grain size deposits (sands), coming in agreement with the outcomes of previous studies where the most prone to lateral deformations areas are the upstream segments (Abayo et al., 2023). In accordance with the expected maximum distance of triggering lateral spreading phenomena from the free face, as recommended by Honegger et al. (2006), Idriss and Boulanger (2008), Youd et al. (2002), Youd (2018), two buffer zones of 50m and 100m were delineated for Orontes river banks. Analyzing the mapped lateral spreading, it was shown that 88.8% of the phenomena were hosted in the former region (50m), while only 11.2% affected the latter one (Table 2).

It should be noted that mud prone areas of finer grain size characteristics should still be classified as likely to liquefaction. This aligns with numerous studies from the past 20 years, which have shown that non-cohesive, low-plasticity silty soils are susceptible to liquefaction (Bray and Sancio, 2006, Idriss and Boulanger, 2008).

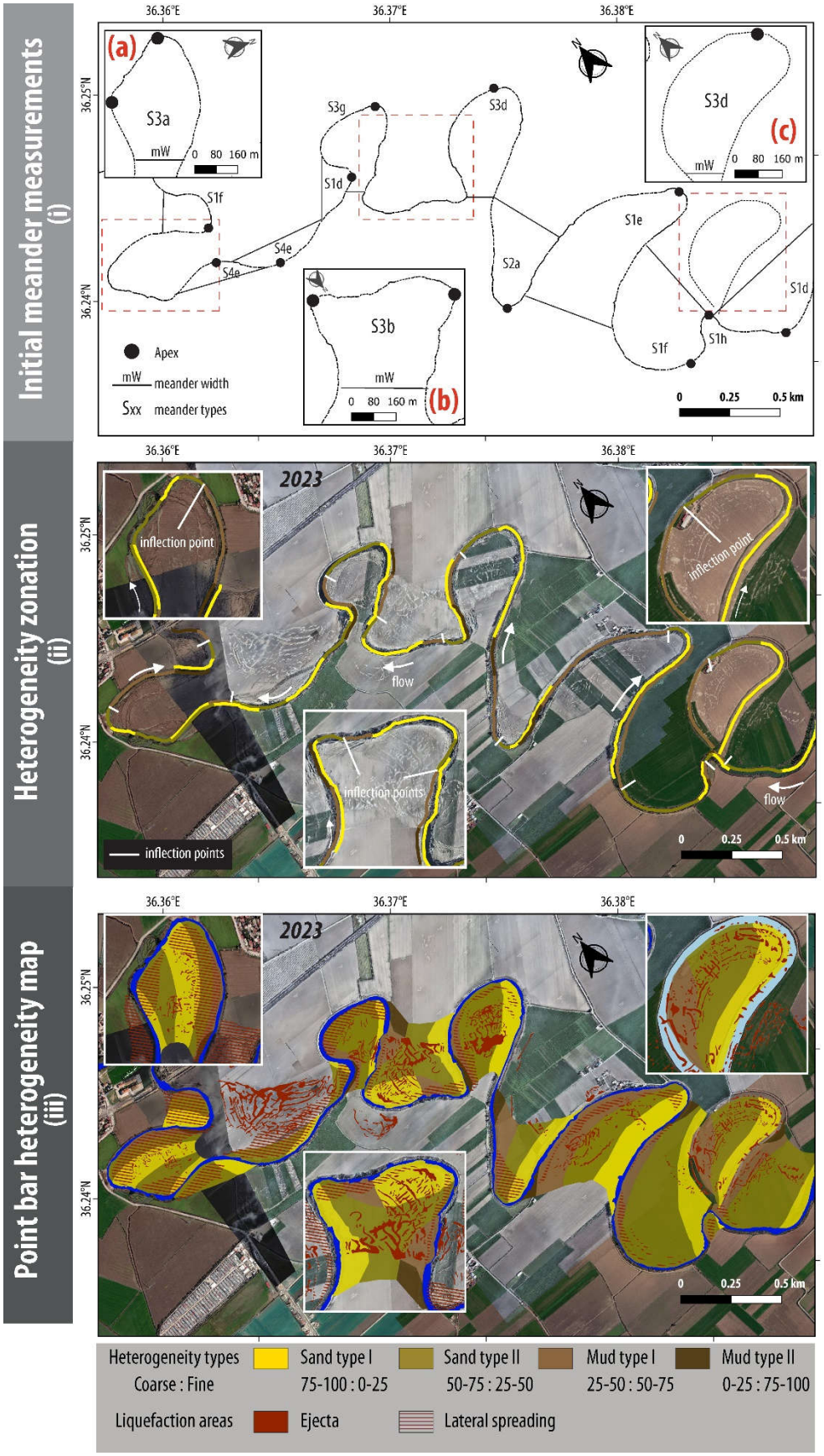

Figure 4. Assessment of heterogeneity types of the Orontes river based on the methodology proposed by Russell (2017). Columns (i-iii) represent the different steps of the procedure for evaluating the sedimentary heterogeneity. Index maps (a, b, c) represent the examples mentioned in this study.

Table 1. Correlation of the spatial distribution of liquefaction sites (%) triggered by the Damasi 2021 earthquake and 2023 Türkiye earthquakes with the relative heterogeneity types of each discussed meander. The total liquefaction percentage corresponds to the spatial distribution of liquefaction phenomena for all the examined cases of Piniada and Orontes Valleys (Fig.3, Fig.4).

		Heterogeneity Type			
		Sand-I	Sand-II	Mud-I	Mud-II
2021 Damasi earthquake	a	13.6	50	33	3.4
	b	63.3	9.4	10.1	17.3
	c	5.0	87.5	7.5	0
	Total liquefaction (%)	38.4	34.3	17.2	10.1
2023 Türkiye earthquakes	a	69.5	30.5	0	0
	b	40.2	51.6	8.2	0
	c	23.5	45.8	30.7	0
	Total liquefaction (%)	24.8	62.7	12.3	0.2

Table 2. Correlation of the spatial distribution of lateral spreading phenomena (%) triggered by 2023 Türkiye earthquakes with the relative heterogeneity types of Orontes River meanders (Fig.4).

		Heterogeneity Type				
	Buffer zones	Sand-I	Sand-II	Mud-I	Mud-II	Total % per buffer zone
Lateral Spreading (%)	50m	12.7	59.4	15.6	1.1	88.8
	100m	5.2	3.4	2.6	0	11.2
	Total % per Type	17.9	62.8	18.2	1.1	

4 Conclusions

The spatial distribution of liquefaction phenomena in Piniada and Orontes Valleys clearly indicates that one of the most susceptible to liquefaction geomorphological features are the point bars formations, which are formed by coarse sediments of sands deposited along the inner bank due to the decreasing flow of meander bend. However, the variable depositional processes along the whole meander results in a complex distribution of lithofacies with alterations between the ratio of coarser and fine materials, which can alterate the preferential behavior of the area to more or less likely to host liquefaction phenomena. Consequently, a detailed mapping of these heterogeneity types would be useful for preliminary geotechnical studies.

For the purposes of this study, point bar features were traced and classified into four heterogeneity classes of Sand-I, Sand-II, Mud-I and Mud-II, based on geological, geomorphological and remote sensing data. Comparison between the spatial distribution of different lithofacies with liquefaction manifestations indicated that most of the effects were triggered in deposits mainly consisted of sandy materials. In particular 72.7% and 87.5% of liquefaction phenomena occurred in Piniada and Orontes respectively, were hosted in Sand-I and Sand-II types of deposits. Highest densities of lateral spreading deformations (72.1%) were also recorded in the same materials in a distance less than 50m from the riverbed. Consequently, it is confirmed that point bar features can further be classified into distinct zones of liquefaction likelihood, improving the forecasting of soil behavior after seismic events and thus minimizing the relevant risk of a manmade environment especially in cases of structural linear works (pipelines, motorways etc.).

Funding
The research activities of D.R. are supported by a contract in the frame of the PON REACT EU Project by the Italian MUR; number 09-G-48651-15.

References

Abayo N.I.; Caba A.C.; Chamberlin E. and Montoya B. Fluvial geomorphic factors affecting liquefaction-induced lateral spreading. *Earthquake Spectra.* 2023. 39, doi: 10.1177/87552930231190655.

Allen J.R.L. A review of the origin and characteristics of recent alluvial sediments. *Sedimentology*, 1965. 5, 89-191, doi: 10.1111/j.1365-3091.1965.tb01561.x.

Bastin S.; Quigley M. and Bassett K. Paleoliquefaction in easter Christchurch, New Zealand. *Geological Society of America bulletin.* 2015, 12, 1348-1365.

Bray J.D; Sancio R.B. Assessment of the liquefaction susceptibility of fine-grained soils. *Journal of Geotechnical and Geoenvironmental Engineering*. 2006, 132: 1165–1177.

Caputo R.; Helly B.; Rapti D. and Valkaniotis S. Late Quaternary hydrographic evolution in Thessaly (Central Greece): The crucial role of the Piniada Valley. *Quaternary International*. 2021. 635, 3-19, doi: 10.1016/j.quaint.2021.02.013.

Carter D.C. 3-D seismic geomorphology: Insights into fluvial reservoir deposition and performance, Widuri field, Java Sea. *AAPG Bulletin*. 2003, 87, 909-934, doi: 10.1306/01300300183.

Civico, R.; Brunori, C.A.; De Martini, P.M.; Pucci, S.; Cinti, F.R.; Pantosti, D. Liquefaction susceptibility assessment in fluvial plains using airborne lidar: The case of the 2012 Emilia earthquake sequence area (Italy). *Natural Hazard Earth System Sciences.* 2015, 15, 2473–2483.

Di Manna P.; Guerrieri L.; Piccardi L.; Vittori E.; Castaldini D.; Berlusconi A.; Bonadeo L.; Comerci V.; Ferrario F.; Gambillara R.; Livio F.; Lucarini M. and Michetti A.M. Ground effects induced by the 2012 seismic sequence in Emilia: implications for seismic hazard assessment in the Po Plain. *Annales geophysicae*. 2012, 55(4), 697-703, doi: 10.4401/ag-6143.

Durkin P.R.; Hubbard S.M.; Boyd R.L. and Leckie D.A. Stratigraphic expression of intra-point-bar erosion and rotation. *Journal of sedimentary research,* 2015. 85, 1238-1257, doi: 10.2110/jsr.2015.78.

Fustic M.; Bennett B.; Huang H. and Larter S. Differential entrapment of charged oil - new insights on McMurray Formation oil trapping mechanisms. *Marine and Petroleum Geology*, 2012. 36(1), 50-69, doi: 10.1016/j.marpetgeo.2012.05.004.

Ghinassi M.; Ielpi A.; Aldinucci M. and Fustic M. Downstream-migrating fluvial point bars in the rock record. *Sedimentary geology*. 2006, 334, 66-96, doi: 10.1016/j.sedgeo.2016.01.005.

Hazir, I.; Akgul, M.A.; Alkaya, M.; Dağdeviren, M.F. From 27 January to 14 March 2012 Evaluation of Floods in Amik Plain of Hatay Province Using Geographic Information Systems. *In Proceedings of the the 4th National Flood Symposium*, Rize, Turkey, 23 November 2016. (In Turkish), 2016.

Honegger D.G.; Nyman D.J.; Youd T.L. Liquefaction Hazard Mitigation for Oil and Gas Pipelines. *In Proceedings of the 100th Anniversary Conference Commemorating the 1906 San Francisco Earthquake*, San Francisco, CA, EERI, 2006.

Idriss I.; Boulanger R. *Soil liquefaction during earthquakes*. Monograph MNO-12, EERI.2008.

Jackson R.G. Sedimentological and fluid-dynamic implications of the turbulent bursting phenomenon in geophysical flows. *Journal of Fluid Mechanics*, 1976. 77(3), 531-560, doi: 10.1017/S0022112076002243.

Miall A.D. Reconstructing the architecture and sequence stratigraphy of the preserved fluvial record as a tool for reservoir development: a reality check. *AAPG Bulletin*. 2006. 90, 989-1002,

Nanson G.C. Point bar and floodplain formation of the meandering Beatton River, Northeastern British Columbia, Canada. Sedimentology, 1980, 27, 3-29, doi: 10.1111/j.1365-3091.1980.tb01155.x.

Nardin T.R.; Howard R.F. and Carter B.J. Stratigraphic architecture of a large-scale point-bar complex in the McMurray Formation: light detection and ranging and subsurface data integration at Syncrude's

Mildred Lake Mine, Alberta, Canada. In: Hein F.J., Leckie D.A. and Suter J.R. (Eds), Heavy oil and oil sand petroleum systems in Alberta and Beyond. *AAPG Bulletin.* 2013. 64, 273-311.

Papathanassiou G.; Caputo R. and Rapti-Caputo D. Liquefaction phenomena along the paleo-Reno River caused by the May 20, 2012, Emilia (northern Italy) earthquake. *Annales geophysicae*, 2012. 55(4), 735-742, doi: 10.4401/ag-6147

Papathanassiou G.; Mantovani A.; Tarabusi G.; Rapti D. and Caputo R. Assessment of liquefaction potential for two liquefaction prone area considering the May 20, 2012 Emilia (Italy) earthquake. *Engineering Geology.* 2015, 189, 1-16, doi: 10.1016/j.enggeo.2015.02.002.

Papathanassiou G.; Valkaniotis S.; Ganas A.; Stampolidis A.; Rapti D. and Caputo R. Floodplain evolution and its influence on liquefaction clustering: the case study of March 2021 Thessaly, Greece, seismic sequence. *Engineering Geology.* 2022, 298, 1-18, doi: 10.1016/j.enggeo.2022.106542.

Russell C.E. Prediction of sedimentary architecture and lithological heterogeneity in fluvial point-bar deposits. PhD thesis, University of Leeds, Leeds, UK, 2017.

Smith D.G.; Hubbard S.M.; Leckie D.A. and Fustic M. Counter point bar Deposits: lithofacies and reservoir significance in the meandering modern Peace River and ancient McMurray Formation, Alberta, Canada. *Sedimentology*, 2009. 56, 1655-1669.

Taftsoglou M.; Valkaniotis S.; Karantanellis S.; Goula E. and Papathanassiou G. Preliminary mapping of liquefaction phenomena triggered by the February 6 2023 M7.7 earthquake, Türkiye / Syria, based on remote sensing data. 2023, doi: 10.5281/zenodo.7668401.

Taftsoglou M.; Valkaniotis S.; Papathanassiou G.; Klimis N. and Dokas I.A. Detailed Liquefaction Susceptibility Map of Nestos River Delta, Thrace, Greece Based on Surficial Geology and Geomorphology. *Geosciences*, 2022. 12, 361, doi: 10.3390/geosciences12100361.

Taftsoglou M.; Valkaniotis S.; Papathanassiou G.; Karantanellis, E. Satellite Imagery for Rapid Detection of Liquefaction Surface Manifestations: The Case Study of Türkiye–Syria 2023 Earthquakes. *Remote Sensing*. 2023. 15, 4190. doi: 10.3390/rs15174190

Thomas R.G.; Smith D.G.; Wood J.M.; Visser J.; Calverley-Range E.A. and Koster E.H. Inclined Heterolithic Stratification-terminology, Description, Interpretation and Significance. *Sedimentary Geology* 1987. 53, 123-179.

Tye R.S. Geomorphology: An approach to determining subsurface reservoir dimensions. *AAPG Bulletin*. 2004. 88(8), 1123-1147, doi: 10.1306/02090403100.

Valkaniotis, S.; Rapti D.; Taftsoglou M.; Papathanassiou G.; Caputo R. Geomorphological mapping for liquefaction likelihood: the Piniada Valley, Greece, case study, *Bulletin of Earthquake Engineering* 2024. (under review)

Wotherspoon L.; Pender M. and Orense R. Relationship between observed liquefaction at Kaiapoi following the 2010 Darfield earthquake and former channels of the Waimakariri River. *Engineering Geology*. 2012, 125, 45-55, doi: 10.1016/j.enggeo.2011.11.001.

Youd T.L. Application of MLR Procedure for Prediction of Liquefaction-Induced Lateral Spread Displacement. *Geotechnical and Geoenvironmental Engineering*. 2018. ASCE, 144(6): 04018033.

Youd T.L.; Hansen C.M.; Bartlett S.F. Revised multilinear regression equations for prediction of lateral spread displacement, *Geotechnical and Geoenvironmental Engineering*. 2002. 128(12): 1007–017.